

PDF hosted at the Radboud Repository of the Radboud University Nijmegen

The following full text is a postprint version which may differ from the publisher's version.

For additional information about this publication click this link.

<http://hdl.handle.net/2066/80003>

Please be advised that this information was generated on 2021-09-23 and may be subject to change.

Chemotherapy response monitoring of colorectal liver metastases by dynamic gadolinium-DTPA enhanced MRI perfusion parameters and FDG-PET metabolic rate

Running title: Response monitoring of liver metastases

Original research

Dennis Vriens, MD*; Hanneke W.M. van Laarhoven, MD, PhD†; Jack J.A. van Asten, MSc‡; Paul F.M. Krabbe, PhD§; Eric P. Visser, PhD*; Arend Heerschap, MD, PhD‡; Cornelis J.A. Punt, MD, PhD†; Lioe-Fee de Geus-Oei, MD, PhD*; Wim J.G. Oyen, MD, PhD*

*Depts. of Nuclear Medicine, †Medical Oncology, ‡Radiology and §Epidemiology, Biostatistics & Health Technology Assessment; Radboud University Nijmegen Medical Centre

Correspondence:

D. Vriens, MD

Department of Nuclear Medicine (internal postal code 444)

Radboud University Nijmegen Medical Centre

P.O. Box 9101, 6500 HB Nijmegen, the Netherlands

Phone: +31-24-3614048, Fax: +31-24-3618942

E-mail: D.Vriens@nucmed.umcn.nl

Word-count all text: 6202 words (max 6,500)

Presented at the SNM 56th Annual Meeting, held at the Toronto Metro Convention Centre, Toronto, Canada, June 15, 2009.

Abstract

In this study, we examined the *in vivo* relationship between functional tumor vasculature, determined by dynamic Gd-DTPA enhanced (DCE-) MRI and tumor metabolism, determined by dynamic [¹⁸F]-fluorodeoxyglucose (FDG-)PET, during cytotoxic treatment of patients with colorectal liver metastases. **Methods:** 23 Patients underwent DCE-MRI and dynamic FDG-PET at baseline and after three treatment cycles unless treatment was terminated due to toxicity. Parameters for vasculature (k_{ep} , K^{trans}), extracellular space (v_e), tumor size (MAD) and metabolism (MR_{glc}) were derived and changes during treatment were correlated. Overall (OS) and progression free (PFS) survival served as outcome measures for the predictive abilities of pre-treatment parameters and of treatment-related parameter changes. **Results:** Pre-treatment MR_{glc} and MAD were individually predictive for OS and PFS. During treatment, K^{trans} increased significantly, but this could not be confirmed in a lesion-by-lesion analysis. MR_{glc} decreased significantly ($p < 0.001$). No correlations were found for changes in DCE-MRI parameters and ΔMR_{glc} . No relation was found between changes in DCE-MRI parameters and OS or PFS. ΔMR_{glc} was able to predict OS ($p = 0.008$) after correction for confounders. **Conclusion:** The efficacy of cytotoxic chemotherapy assessed by reduction in tumor metabolism does not depend on pre-treatment properties of the tumor vasculature determined by DCE-MRI. Cytotoxic chemotherapy does not alter DCE-MRI-derived properties of tumor vasculature, but decreases glucose consumption of tumor cells.

Keywords: Colorectal carcinoma – DCE-MRI – [¹⁸F]FDG – Positron emission tomography – chemotherapy – therapy monitoring – survival

Introduction

Chemotherapy is usually the treatment of choice in patients with advanced colorectal cancer (CRC). Advances in cytotoxic treatment have improved the median survival from eight to more than 20 months (1). Unfortunately, chemotherapy is only effective in a subset of patients. Early response prediction would enable individualized treatment and prevent side effects and costs due to futile treatment of non-responders.

The efficacy of chemotherapy depends on the delivery of cytotoxic drugs by the tumor vasculature, on uptake and retention of the drug in tumor cells, on metabolic activation of prodrugs, on intrinsic chemosensitivity of tumor cells and on catabolism and excretion of drugs. Capillary perfusion and permeability of the vessel wall can be measured *in vivo* by dynamic gadopentetate dimeglumine (Gd-DTPA) contrast-enhanced magnetic resonance imaging (DCE-MRI) (2). Glucose metabolic activity can be assessed *in vivo* by positron emission tomography (PET) using the radionuclide labeled glucose-analogue [¹⁸F]-fluoro-2-deoxy-D-glucose (FDG) (3).

Pharmacokinetic analysis of DCE-MRI data yields parameters for perfused capillaries including blood flow, permeability and the total surface area. Assuming that vascularity, as reflected by these parameters, is also relevant for delivery of relatively small cytotoxics to the tumor, it may be hypothesized that these parameters can be used for prediction of treatment response. The value of baseline DCE-MRI parameters to predict treatment outcome has been shown for several tumor types including CRC (4, 5) and its significance in early monitoring of treatment response has been shown for rectal (5) and breast (6-8) cancer.

FDG uptake is increased in malignant tumors. An adequate vascular supply is necessary for delivery of glucose to tumor cells as well as the presence of several membrane bound glucose transport proteins and intracellular hexokinase for subsequent phosphorylation. FDG uptake can be quantified by glucose metabolic rates (MR_{glc}) derived

from dynamic FDG-PET data. The value of baseline MR_{glc} as a predictive parameter for treatment outcome has been shown for several tumor types, including non-small cell lung carcinoma (NSCLC) and CRC (9) and its predictive value for early evaluation of treatment response, using changes in MR_{glc} during (chemo)therapy, has been shown in many tumor types including NSCLC (10) and CRC (11).

As DCE-MRI and FDG-PET assess two different determinants of chemotherapy efficacy, their combination could aid in the unraveling of the principles of chemosensitivity. In this prospective study, we investigated the predictive value of pre-treatment pharmacokinetic parameters and the value of (early) cytotoxic therapy-induced changes in pharmacokinetic parameters of Gd-DTPA and FDG with respect to overall (OS) and progression free survival (PFS).

Materials and methods

Patients

Between June 2002 and September 2005, patients with liver metastases of histologically proven CRC who underwent a diagnostic work-up before start of cytotoxic chemotherapy were eligible. Liver metastases were established during routine staging or during follow-up by abdominal CT (n=21), ultrasound (n=1) or MRI (n=1). Follow-up included a three-monthly ultrasonography or CT-scan. Patients with diabetes mellitus, severe claustrophobia or with implanted electrical devices were excluded as well as patients with (multiple) small (<1 cm) lesions, in whom the limited spatial resolution of the PET-scanner would pose technical difficulties for quantification. The study was approved by the institutional review board of the Radboud University Nijmegen Medical Centre and all patients gave written informed consent.

Thirty-three patients with liver metastases of CRC were included in this prospective study. For five patients DCE-MRI data were not complete due to technical problems (n=2), unavailability of a pre-therapy scan (n=1) or follow-up scan (n=2) and for four patients FDG-PET data were not complete due to technical problems during the follow-up dynamic acquisition (n=1) or unavailability of a follow-up scan (n=3). For one patient both DCE-MRI and FDG-PET at follow-up were inaccessible. Therefore, complete datasets of two DCE-MRIs and two FDG-PETs were available for 23 patients for analysis of treatment response. Patient characteristics are listed in table 1. Thirty-one lesions in total could be matched for lesion-by-lesion analysis on MRI (34 lesions visible) and FDG-PET (56 lesions visible, due to the larger axial field of view (FoV) of PET compared to MRI) by experienced observers (L.F.d.G.O. and H.W.M.v.L.). In four patients, metastases visible on DCE-MRI could not be identified as separate lesions on FDG-PET. Therefore, the MR_{glc} of the combined lesion was used.

Nine patients received chemotherapy in first line, eleven in second, two in third and one patient in fourth line. The median interval between the last day of previous line chemotherapy and the baseline scan for patients treated in 2nd or higher line was 39 days (IQR: 23-150 days). None of these fourteen patients had been treated with anti-angiogenic agents before inclusion. The treatment regimens were: irinotecan (n=7), capecitabine (n=5), capecitabine / irinotecan (n=4), capecitabine / oxaliplatin (n=3), 5-fluorouracil (5-FU) / folinic acid (FA) / oxaliplatin (FOLFOX, n=3) and 5-FU / FA (n=1).

No patients were lost to follow-up. Median overall survival was 1.5 years (1-, 2- and 3-year proportions: 70%, 26% and 9%, respectively) and median progression free survival was 5.3 months. At the closeout date, two patients were alive (follow-up 4.3 and 5.6 years, respectively). All patients showed progression of disease.

DCE-MRI and FDG-PET were performed before start and after 3 cycles of chemotherapy (cycle duration 21 days except for FOLFOX, which has a cycle duration of 14 days). When treatment had been terminated before 3 cycles (n=6, range: 0.5-2.0 cycles)

the follow-up scan was performed earlier. The median duration of treatment was 50 days (IQR: 30-56 days). The median interval between last treatment day and follow-up scan was 6 days (IQR: 2.5-15.5 days).

DCE-MRI

Quantitative DCE-MRI data acquisition and reconstruction

Measurements were performed on a 1.5 T Siemens MR scanner, using a body phased array coil. After conventional T₁- and T₂-weighted imaging, 15 mL 0.5 M Gd-DTPA (Magnevist®, Schering, Berlin, Germany) was administered intravenously at an injection rate of 2.5 mL·s⁻¹ by a Spectris™ MR injection system (Medrad Inc., Maastricht, the Netherlands). An axial T₁-weighted fast low-angle shot (FLASH) sequence was used to monitor Gd-DTPA uptake in the tumor and the bolus passage in vessels in the spleen (repetition time (TR) 21 ms, echo time (TE) 1.5-1.57 ms, flip angle 45°, slice thickness 7 mm, 4 to 6 slices, matrix size 256·125 pixels, FoV 284·350 mm, total acquisition time 90 s). The fast acquisition scheme was performed multi-slice, *i.e.* 4-6 slices were acquired simultaneously within the TR, realized by short TE and short pulse duration. The acquisition matrix was 256·125 pixels per slice. Application of the Partial Fourier technique (factor 6/8) reduced the number of phase encoding steps to 94, which in turn led to a net temporal resolution of $94 \cdot \sim 21 \text{ ms} = \sim 2 \text{ seconds}$. If the four to six slices in the axial FoV did not fully cover the tumor in the axial direction, slices were positioned in such a way that the largest diameter of the tumor (on the coronal view) was covered. During the acquisition patients were instructed to perform quiet and shallow breathing.

Immediately prior to Gd-DTPA injection, proton density weighted images were recorded with the same sequence parameters as the DCE-MRI except for a flip angle of 10° and a TR of 250 ms. Data from these images were combined with the DCE-MRI data to

calculate the concentration of Gd-DTPA in arbitrary units, using the methods described by Hittmair *et al.* (12).

MRI data analysis

For the analysis of DCE-MRI a vascular normalization function was obtained from pixels in the spleen using an algorithm based on the concentration of Gd-DTPA (high in blood vessels) and time to bolus passage (short in arteries) as described earlier (13). Using a physiological pharmacokinetic model (14) the Gd-DTPA concentration versus time curves of the pixels in all MRI slices, (256·125 pixels), containing tumor tissue were analyzed and values of the rate constant k_{ep} (s^{-1}) of Gd-DTPA uptake were calculated according to the formula: $c_t(t) = K^{trans} \cdot e^{-k_{ep}t} \otimes c_p(t)$, in which c_t is the tissue concentration of Gd-DTPA; k_{ep} is the rate constant of contrast agent exchange between the extracellular extravascular space and the plasma compartment; K^{trans} is the volume transfer constant between these compartments (s^{-1}); c_p is the concentration of contrast agent in plasma of a capillary and “ \otimes ” denotes a convolution operation (2). In Larsson’s model (14), the Gd-DTPA uptake rate constant (k_{ep}) is directly related to tumor blood flow, the product of the permeability and the total surface area of perfused capillaries, according to: $k_{ep} = (1 - e^{-P \cdot S \cdot TBF^{-1}}) \cdot TBF \cdot v_e^{-1} = K^{trans} \cdot v_e^{-1}$, in which v_e is the volume of extravascular extracellular space per unit volume of tissue; P is the permeability of capillaries ($cm \cdot s^{-1}$); S is the total surface area of the vessels (cm^2) and TBF is the tumor blood flow ($mL \cdot s^{-1}$). Previous reports have confirmed that there is a moderately strong positive correlation between k_{ep} and microvessel density in liver metastases ($r=0.458$, $p=0.037$) (15).

The spatial distribution of the pharmacokinetic parameters were represented as a map. On a T_1 -weighted MR image recorded directly before Gd-DTPA injection a region of interest (RoI) was drawn which comprised the metastases. Only large lesions (i.e. >15 mm),

that were totally covered by the FoV of the acquired images and were not disturbed by artifacts of inflow of Gd-DTPA in the abdominal aorta (i.e. lesions directly ventral to the aorta) were included. Six lesions were smaller than 30 mm. This RoI was applied to the map of pharmacokinetic parameters in order to select the single values of k_{ep} , K^{trans} and v_e for all tumor pixels. Whole-tumor values were calculated after log transformation of all voxels within the RoI, thereby excluding voxels for which k_{ep} , K^{trans} and $v_e = 0 \text{ s}^{-1}$, which are assumed to represent necrotic tissue or fit artifacts. Mean tumor values and 95% confidence intervals (CI) were obtained by back transformation (13). To obtain a whole-patient value, a mean value, weighted by lesion volume, of all lesions within the FoV was determined by:

$$parameter_{whole-patient} = \sum (parameter_{lesion} \cdot volume_{lesion}) / \sum volume_{lesion}$$

The coronal T₁-weighted images were used to measure the maximal axial diameter of each included lesion (MAD, in mm) in order to evaluate morphological treatment response. Patient-based MADs were calculated by the sum of all included lesions.

FDG-PET

Quantitative dynamic FDG-PET data acquisition and reconstruction

Dynamic PET was performed on a Siemens ECAT-EXACT 47 dedicated PET-scanner (Siemens/CTI, Knoxville, TN, USA) using the ECAT 7.2.1 software for 2D reconstruction. Patients fasted for at least six hours prior to imaging. Intake of sugar-free liquids was permitted. Blood glucose levels (hexokinase method, Aerose, Abbott diagnostics, IL, USA) were determined. Median fasting glucose was 5.3 mmol.L^{-1} (maximum: 9.2 mmol.L^{-1}). The location for the dynamic acquisition in the scanners axial field of view (FoV, 162 mm in 47 planes) was based on whole-body FDG-PET and CT scans performed for routine clinical work-up, including as many measurable tumor lesions as possible. A 20-min transmission scan was made, using the internal $^{68}\text{Ge}/^{68}\text{Ga}$ sources, to correct for photon

attenuation. Approximately 200 MBq (mean: 202 ± 40 MBq) FDG (Covidien, Petten, the Netherlands) was injected intravenously using constant infusion by a remote-controlled pump (Medrad Inc., Indianola, PA, USA). The dynamic data acquisition, performed in 2-dimensional mode, was started simultaneously with the injection of FDG and consisted of 16 timeframes with variable duration (10-30 s, 3-300 s, 3-600 s) for a total time of 50 minutes. During the acquisition patients were instructed to perform quiet and shallow breathing. Correction for decay, randoms, and scatter was performed. Attenuation-corrected images were reconstructed in $128 \cdot 128$ matrices using filtered back projection with a Gaussian filter of 4 mm FWHM (full width at half maximum). This resulted in $47 \cdot 3.375$ mm slices for each timeframe, with voxel dimensions of $3.432 \cdot 3.432 \cdot 3.375$ mm and a spatial resolution of 6 mm FWHM in the reconstructed images.

FDG-PET data analysis

The analysis of FDG-PET data, was performed as described before (16). In brief, a plasma time-activity concentration curve was obtained by serial arterial sampling. When arterial sampling was not feasible or contra-indicated, an image-derived input function (IDIF) of the abdominal aorta was used (48% of 46 FDG-PET scans). Tumor time-activity concentration curves were obtained by determination of volume weighted mean activity concentration within regions of interest (RoI). These RoIs were placed semi-automatically over the metastases using 50% of the maximum voxel value within the lesion on the summed images of frames 14-16 (20-50 min post injection). For therapy response monitoring, the lesion-specific RoI with largest volume was copied to the other scan (17). Using Patlak graphical analysis (3, 18) glucose metabolic rates (MR_{glc}) were determined, using a lumped constant of 1 and a fractional blood volume of 0. A volume-weighted mean value for all lesions corresponding with DCE-MRI was obtained as patient-based data using the same equation as for DCE-MRI data.

Clinical Follow-Up

Follow-up was performed according to a stringent protocol for three years according to standard clinical care. Tumor response for clinical decision-making was evaluated by experienced radiologists according to RECIST-criteria (19) without knowledge of DCE-MRI or dynamic FDG-PET results. Changes in DCE-MRI parameters (k_{ep} , K^{trans} , v_e), MAD and the FDG-PET parameter MR_{glc} during treatment, were calculated as:

$$\Delta parameter = (parameter_{follow-up} - parameter_{baseline}) \cdot parameter_{baseline}^{-1} \cdot 100\%$$

The date of progression was defined as the earliest date at which disease progression was confirmed. Survival and progression were measured from the date of baseline FDG-PET or DCE-MRI (whichever was performed first) to the date of respectively disease-related death or progression. For patients who were alive (n=2) at the closeout date (May 2009), survival was censored.

Median interval between all DCE-MRIs and FDG-PETs was 0 days (IQR 0-1 days). Mean interval between baseline and the first follow-up PET-scan was 59.1 ± 11.3 days.

Statistical Analysis

Both patient-based analysis and lesion-by-lesion analysis were performed. Analysis of DCE-MRI, T₁-MRI and FDG-PET were performed separately and the results were blinded. Variables were assessed for normality by Shapiro-Wilk statistics. Means (\pm SD) for normal distributed data or medians (interquartile range, IQR) are presented. Differences were assessed for significance by the Mann-Whitney U test and by the paired t-test (normally distributed) or Wilcoxon signed ranks test for paired data. Correlations were determined by the non-parametric Spearman's ρ .

Cancer related overall survival (OS) and progression free survival (PFS) were calculated using Kaplan-Meier estimates. Both univariate- and multivariate analysis was performed by the Cox proportional hazards model. The relation between DCE-MRI and

FDG-PET parameters and OS and PFS was assessed for both pre-treatment values (predictive value of tumor parameters) and changes in parameter values during treatment (predictive value of early treatment response). Separate (univariate) analysis was performed for the relation between OS / PFS and the following covariates: number of lesions, patient age, TNM-classification, tumor differentiation, histology or localization, chemotherapy line (first line versus 2nd or higher line) and regimen and the number of chemotherapy cycles before the follow-up scan. Hazard ratios (HR) are presented with their 95% confidence intervals (Wald's χ^2 test). Multivariate analysis was performed using imaging parameters and significant covariates in a backwardly designed conditional Cox proportional hazards model, removing variables when $p > 0.100$.

All statistical analyses were performed with SPSS® version 16.0.2 for Mac (SPSS Inc., Chicago, Illinois, USA). Statistical tests were based on a two-sided significance level set at $p = 0.050$ for all tests.

Results

Predictive value of pre-treatment DCE-MRI and FDG-PET

An example of DCE-MRI and FDG-PET data is displayed in figure 1. No statistically different pre-treatment parameters for tumor size and vascular parameters were found for patients who were treated in first line ($n = 9$) versus patients who had been treated with cytotoxic therapy previously ($n = 14$). Glucose metabolic rate was slightly lower in the patients that were treated in first line. This, however, did not reach significance (median $MR_{glc} = 0.1095 \mu\text{mol} \cdot \text{mL}^{-1} \cdot \text{min}^{-1}$ versus $0.1373 \mu\text{mol} \cdot \text{mL}^{-1} \cdot \text{min}^{-1}$, $p = 0.072$).

Patient based analysis of the pre-treatment scans showed a significant positive correlation between tumor size (MAD) and fraction of extravascular extracellular space (v_e) ($\rho = 0.426$, $p = 0.043$). Neither the patient-base analysis nor the lesion-by-lesion analysis

yielded significant correlations between pre-treatment DCE-MRI and FDG-PET parameters. The correlation between baseline k_{ep} and MR_{glc} was -0.028 ($p=0.880$).

Univariate Cox regression analysis established an OS and PFS benefit in patients with a low baseline MR_{glc} values. Baseline MAD showed a minor but significant relation with OS as well, but chemotherapy line (1st line versus higher lines) showed no significant relation with either OS or PFS in this group of patients. None of the DCE-MRI parameters for vascularity showed a significant relation with either OS or PFS. When these variables were used in multivariate analysis, correction for MAD increased the HR of MR_{glc} for OS and PFS, but additional correction for chemotherapy line did not improve the predictive ability of the model as a whole (table 2).

Lesion-by-lesion analysis of changes in scan parameters:

A significant change in median MR_{glc} ($0.138 \mu\text{mol}\cdot\text{mL}^{-1}\cdot\text{min}^{-1}$ to $0.059 \mu\text{mol}\cdot\text{mL}^{-1}\cdot\text{min}^{-1}$, $p<0.001$) was found at the follow-up but no significant changes were seen in the other parameters. K^{trans} did not change significantly ($p=0.088$). No correlations were present between changes in FDG-PET parameters and changes in DCE-MRI parameters during treatment.

Predictive value of changes in DCE-MRI and FDG-PET parameters

For response to chemotherapy, no statistical differences were seen between the changes in tumor size, DCE-MRI vascularity parameters and MR_{glc} , between the group that was treated with systemic treatment in first line ($n=9$) and the group that was treated in higher ($n=14$) lines (all $p>0.305$).

Results of scan parameters before and after start of treatment are provided in table 3. There was a significant change in both MR_{glc} (median baseline $0.128 \mu\text{mol}\cdot\text{mL}^{-1}\cdot\text{min}^{-1}$ to

0.054 $\mu\text{mol}\cdot\text{mL}^{-1}\cdot\text{min}^{-1}$ at follow-up, $p<0.001$) and K^{trans} (median baseline 0.009 s^{-1} to 0.016 s^{-1} at follow-up, $p=0.035$) during chemotherapy. No significant correlations were found between parameter changes during treatment. The correlation between ΔK^{trans} and $\Delta\text{MR}_{\text{glc}}$ was $\rho=-0.172$ ($p=0.433$).

To assess whether pre-existing vasculature as assessed by DCE-MRI influenced therapy response by delivery of cytotoxic drugs, k_{ep} prior to chemotherapy was correlated to metabolic and anatomical response, but no significant relation could be established between k_{ep} and ΔMAD ($\rho=-0.209$, $p=0.340$) or $\Delta\text{MR}_{\text{glc}}$ ($\rho=0.257$, $p=0.237$). The same applied for K^{trans} and v_e . In lesion-by-lesion analysis, k_{ep} prior to chemotherapy was not correlated with ΔMAD ($\rho=-0.197$, $p=0.289$) or $\Delta\text{MR}_{\text{glc}}$ ($\rho=0.293$, $p=0.109$).

Univariate Cox regression analysis showed no relation of any change in DCE-MRI or FDG-PET parameters with respect to OS. When all lesions inside the larger PET-scanner's FoV were quantified (instead of only the matching lesions) to determine a patient-based MR_{glc} , $\Delta\text{MR}_{\text{glc}}$ was predictive for OS (HR=1.15, $p=0.041$). Only ΔMAD was related to both OS (HR=1.40, $p=0.023$) and PFS (HR=1.34, $p=0.026$). Chemotherapy line was not a significant confounder for OS or PFS. Multivariate Cox regression modeling showed both $\Delta\text{MR}_{\text{glc}}$ (HR=1.22, $p=0.008$) and Δk_{ep} (HR=0.99, $p=0.100$) as predictors for OS, but the latter was irrelevantly small. For PFS both ΔMAD (HR=1.48, $p=0.010$) and chemotherapy line (HR=3.15, $p=0.023$) were of predictive relevance. Results are shown in table 4.

Discussion

Pre-treatment parameters for vascularity and metabolism

No association was seen between vascularity, assessed by DCE-MRI and glucose metabolism, assessed by FDG-PET. Our results confirm those of Brix *et al.* (20), who

found no correlation between k_{ep} and FDG uptake (standardised uptake value, SUV) in breast cancer. Semple *et al.* (21), however, found a positive correlation between k_{ep} and SUV ($\rho=0.5$) and a positive, though non-significant correlation between K^{trans} and SUV in breast carcinoma patients before commencement of treatment. They suggest that FDG delivery is restricted by the blood flow dynamics of the tumor. In a previous study (15), we found a negative correlation between k_{ep} and FDG uptake (tumor to non-tumor ratios) in CRC.

The different relations between vascular and metabolic tumor parameters described in literature could imply that tumor vasculature is not related to MR_{glc} . However, a more complex relation between vasculature and MR_{glc} , mediated by acute and chronic tumor hypoxia, could also play a role: chronic hypoxia and diminished delivery of glucose could be caused by a low blood flow, a low permeability, and/or a small surface area of tumor blood vessels resulting in low values for k_{ep} . All these vascular parameters may result in a decreased supply of nutrients like glucose and oxygen to the tumor similar to the decreased delivery of Gd-DTPA, which would lead to decreased cell proliferation as an energy saving method (22) or to necrosis or apoptosis. This situation would result in a positive correlation between k_{ep} and MR_{glc} . Conversely, (transient) hypoxia due to poor vascular function (as measured by a low value for k_{ep}) might induce higher glucose uptake in the tumor for anaerobic glycolysis (15, 23, 24). The latter explanation would result in a negative correlation between k_{ep} and MR_{glc} . Therefore, the opposite, combined, complex effects of acute and chronic hypoxia and nutrient supply could explain the lack of correlation between k_{ep} and MR_{glc} . Another reason for this lack of correlation could be non-specificity of K^{trans} and k_{ep} , which may represent flow, vessel permeability or surface area or a combination of these. Finally, imprecision in the determination of the DCE-MRI- and/or PET-parameters combined with the limited study size, might explain the lack of correlation.

Both pre-treatment tumor metabolism (MR_{glc}) and size (MAD) were associated with higher hazards for death and progression. This confirms previous data (9), which showed

that a one unit increase in SUV, results in a 17% increase in the risk of death. Multivariate analysis showed no influence of chemotherapy line (first versus higher line treatment) for the predictive abilities of MR_{glc} and MAD.

Previously, Semple *et al.* (25) had observed a significant correlation ($p < 0.05$) between pre-treatment k_{ep} and ΔSUV during chemotherapy of 17 breast cancer patients and concluded that reduction of measured metabolism may be partly attributable to pre-therapy vascular delivery (k_{ep}). Since Gd-DTPA is similarly distributed in the interstitium of tumor tissue as phenylacetate (26) (which has similar size as 5-FU), a restriction of Gd-DTPA delivery to the interstitium reflects a restriction of 5-FU delivery to the immediate neighborhood of tumor cells. We could not confirm these findings in patients with CRC.

(Early) changes in metabolic and vascularity parameters during treatment

We have found no significant treatment induced changes in k_{ep} , V_e and MAD, whereas MR_{glc} and K^{trans} , respectively, significantly decreased and increased on patient level. On lesion level, the increase in K^{trans} could not be reproduced. Our results suggest that the observed reduction in MR_{glc} during chemotherapy cannot be explained by changes in tumor vasculature (Δk_{ep}). The antivascular effect of cytotoxic drugs is small and marginally influences cell metabolism and patient survival. It seems that direct cytotoxic effects leading to necrosis and apoptosis cause disease response and improved survival and that possible effects of chemotherapeutic agents on nutrient delivery play a minor role.

Reduction in k_{ep} during therapy has been described in breast cancer (27, 28) and reduction in K^{trans} during treatment has been described in rectal (5) and breast (6, 7, 29) cancer. Some authors explain these changes by the direct antivascular effect of the cytotoxic drugs (7, 29) or by the loss of immature tumor vessels (5). Our results, however, do not suggest an effect of cytotoxic drugs on tumor vasculature in CRC.

We found no relation between vascular parameters and clinical outcome. This confirms the results of our previous study showing no evident relevance of pre-treatment k_{ep} , K^{trans} or v_e for OS and PFS in colorectal liver metastases or any change in these parameters during first line chemotherapy (30). In the present study, we observed a positive relation between ΔMR_{glc} and hazards for death but not for progression, which was mainly predicted by chemotherapy line and ΔMAD .

Since DCE-MRI and FDG-PET both address different aspects of tumor physiology, they might be used complementary in treatment response evaluation. The choice for a specific imaging modality should depend on the treatment regimen. The cytotoxic drugs given to our patients interfere with DNA-synthesis and -stabilization, eventually leading to cell-death. Therefore, direct interaction with tumor vascularity is limited, as is suggested by our data, showing no change in DCE-MRI parameters during cytotoxic treatment. When anti-angiogenic drugs are used, response might be predicted by DCE-MRI as shown by two studies (31, 32) in clear cell renal cell carcinoma patients treated with sorafenib. Response might be monitored by DCE-MRI, showing a decrease of k_{ep} (33), but results are still contradictory (32). The effect of cytotoxic drugs on cell metabolism can be monitored by FDG-PET. Tumor metabolic response has predictive value (11), which is also shown by our data. Of note, early disease related deaths did occur in the group of metabolic responders. Therefore, a reduction in metabolism during therapy does not guarantee a long survival and more effects presumably play a role.

Study Limitations

The included population is heterogeneous as patients were treated in different lines of chemotherapy using different chemotherapy regimens. Furthermore, nowadays combinations of cytotoxic treatment with anti-angiogenic treatment are standard in first line. DCE-MRI may have a role as a tool for response evaluation in those patients who are

being treated with anti-angiogenic therapy. Previous chemotherapy might already have influenced both metabolism and vascularity. However, subgroup analysis of the nine patients treated with first line chemotherapy did not change our conclusions.

Only a selection of lesions could be analyzed due to the limited FoV of the acquired images and the limited spatial resolution of (especially) the PET system, which might have caused some bias during selection.

The parameters for vascularity as derived from DCE-MRI were not verified by histological quantification of microvessel density as biopsies of stage IV patients are only taken in exceptional circumstances. However, we have previously described a relation between both histology and DCE-MRI parameters (15). An advantage of DCE-MRI over histology is that DCE-MRI measures functional vasculature only while quantification of histological staining of endothelial cells also includes non-perfused vessels.

Conclusion

Dynamic Gd-DTPA enhanced MRI parameters of tumor vasculature showed no relation to tumor metabolic response on dynamic FDG-PET or to patient survival during cytotoxic chemotherapy neither before nor during treatment. Therefore, a decrease in metabolic activity and increase in OS and PFS during chemotherapy cannot be attributed to changes in tumor vascularity, resulting in altered delivery of drugs or nutrients of the same size as Gd-DTPA. The present study underlines the potential of FDG-PET for response monitoring. The main conclusions of the paper are valid for patients not receiving vascular-targeted therapy, while further study is required in the subset of patients who do receive additional anti-angiogenic agents.

Reference List

1. Punt CJ. New options and old dilemmas in the treatment of patients with advanced colorectal cancer. *Ann Oncol.* 2004;15:1453-1459.
2. Tofts PS, Brix G, Buckley DL, et al. Estimating kinetic parameters from dynamic contrast-enhanced T(1)-weighted MRI of a diffusable tracer: standardized quantities and symbols. *J Magn Reson Imaging.* 1999;10:223-232.
3. Patlak CS, Blasberg RG, Fenstermacher JD. Graphical evaluation of blood-to-brain transfer constants from multiple-time uptake data. *J Cereb Blood Flow Metab.* 1983;3:1-7.
4. Devries AF, Griebel J, Kremser C, et al. Tumor microcirculation evaluated by dynamic magnetic resonance imaging predicts therapy outcome for primary rectal carcinoma. *Cancer research.* 2001;61:2513-2516.
5. George ML, Dzik-Jurasz AS, Padhani AR, et al. Non-invasive methods of assessing angiogenesis and their value in predicting response to treatment in colorectal cancer. *The British journal of surgery.* 2001;88:1628-1636.
6. Pickles MD, Lowry M, Manton DJ, Gibbs P, Turnbull LW. Role of dynamic contrast enhanced MRI in monitoring early response of locally advanced breast cancer to neoadjuvant chemotherapy. *Breast cancer research and treatment.* 2005;91:1-10.
7. Delille JP, Slanetz PJ, Yeh ED, Halpern EF, Kopans DB, Garrido L. Invasive ductal breast carcinoma response to neoadjuvant chemotherapy: noninvasive monitoring with functional MR imaging pilot study. *Radiology.* 2003;228:63-69.
8. Thukral A, Thomasson DM, Chow CK, et al. Inflammatory breast cancer: dynamic contrast-enhanced MR in patients receiving bevacizumab--initial experience. *Radiology.* 2007;244:727-735.
9. de Geus-Oei LF, Wiering B, Krabbe PF, Ruers TJ, Punt CJ, Oyen WJ. FDG-PET for prediction of survival of patients with metastatic colorectal carcinoma. *Ann Oncol.* 2006;17:1650-1655.
10. de Geus-Oei LF, van der Heijden HF, Visser EP, et al. Chemotherapy response evaluation with 18F-FDG PET in patients with non-small cell lung cancer. *J Nucl Med.* 2007;48:1592-1598.
11. de Geus-Oei LF, van Laarhoven HW, Visser EP, et al. Chemotherapy response evaluation with FDG-PET in patients with colorectal cancer. *Ann Oncol.* 2008;19:348-352.
12. Hittmair K, Gomiscek G, Langenberger K, Recht M, Imhof H, Kramer J. Method for the quantitative assessment of contrast agent uptake in dynamic contrast-enhanced MRI. *Magn Reson Med.* 1994;31:567-571.

13. van Laarhoven HW, Rijpkema M, Punt CJ, et al. Method for quantitation of dynamic MRI contrast agent uptake in colorectal liver metastases. *J Magn Reson Imaging*. 2003;18:315-320.
14. Larsson HB, Stubgaard M, Frederiksen JL, Jensen M, Henriksen O, Paulson OB. Quantitation of blood-brain barrier defect by magnetic resonance imaging and gadolinium-DTPA in patients with multiple sclerosis and brain tumors. *Magn Reson Med*. 1990;16:117-131.
15. van Laarhoven HW, de Geus-Oei LF, Wiering B, et al. Gadopentetate dimeglumine and FDG uptake in liver metastases of colorectal carcinoma as determined with MR imaging and PET. *Radiology*. 2005;237:181-188.
16. de Geus-Oei LF, Visser EP, Krabbe PF, et al. Comparison of image-derived and arterial input functions for estimating the rate of glucose metabolism in therapy-monitoring 18F-FDG PET studies. *J Nucl Med*. 2006;47:945-949.
17. Vriens D, de Geus-Oei LF, van Laarhoven HWM, et al. Comparison of two region of interest definition methods for metabolic response evaluation with [18F]FDG-PET. *Q J Nucl Med Mol Imaging*. 2009;in press.
18. Willemsen AT, van den Hoff J. Fundamentals of quantitative PET data analysis. *Curr Pharm Des*. 2002;8:1513-1526.
19. Therasse P, Arbuck SG, Eisenhauer EA, et al. New guidelines to evaluate the response to treatment in solid tumors. European Organization for Research and Treatment of Cancer, National Cancer Institute of the United States, National Cancer Institute of Canada. *Journal of the National Cancer Institute*. 2000;92:205-216.
20. Brix G, Henze M, Knopp MV, et al. Comparison of pharmacokinetic MRI and [18F] fluorodeoxyglucose PET in the diagnosis of breast cancer: initial experience. *European radiology*. 2001;11:2058-2070.
21. Semple SI, Gilbert FJ, Redpath TW, et al. The relationship between vascular and metabolic characteristics of primary breast tumours. *European radiology*. 2004;14:2038-2045.
22. Evans SM, Hahn SM, Magarelli DP, Koch CJ. Hypoxic heterogeneity in human tumors: EF5 binding, vasculature, necrosis, and proliferation. *American journal of clinical oncology*. 2001;24:467-472.
23. Burgman P, Odonoghue JA, Humm JL, Ling CC. Hypoxia-Induced increase in FDG uptake in MCF7 cells. *J Nucl Med*. 2001;42:170-175.
24. Clavo AC, Brown RS, Wahl RL. Fluorodeoxyglucose uptake in human cancer cell lines is increased by hypoxia. *J Nucl Med*. 1995;36:1625-1632.
25. Semple SI, Staff RT, Heys SD, et al. Baseline MRI delivery characteristics predict change in invasive ductal breast carcinoma PET metabolism as a result of primary chemotherapy administration. *Ann Oncol*. 2006;17:1393-1398.

26. Artemov D, Solaiyappan M, Bhujwala ZM. Magnetic resonance pharmacangiography to detect and predict chemotherapy delivery to solid tumors. *Cancer research*. 2001;61:3039-3044.
27. Wasser K, Klein SK, Fink C, et al. Evaluation of neoadjuvant chemotherapeutic response of breast cancer using dynamic MRI with high temporal resolution. *European radiology*. 2003;13:80-87.
28. Wasser K, Sinn HP, Fink C, et al. Accuracy of tumor size measurement in breast cancer using MRI is influenced by histological regression induced by neoadjuvant chemotherapy. *European radiology*. 2003;13:1213-1223.
29. Hayes C, Padhani AR, Leach MO. Assessing changes in tumour vascular function using dynamic contrast-enhanced magnetic resonance imaging. *NMR in biomedicine*. 2002;15:154-163.
30. van Laarhoven HW, Klomp DW, Rijpkema M, et al. Prediction of chemotherapeutic response of colorectal liver metastases with dynamic gadolinium-DTPA-enhanced MRI and localized ¹⁹F MRS pharmacokinetic studies of 5-fluorouracil. *NMR in biomedicine*. 2007;20:128-140.
31. Flaherty KT, Rosen MA, Heitjan DF, et al. Pilot study of DCE-MRI to predict progression-free survival with sorafenib therapy in renal cell carcinoma. *Cancer Biol Ther*. 2008;7:496-501.
32. Hahn OM, Yang C, Medved M, et al. Dynamic contrast-enhanced magnetic resonance imaging pharmacodynamic biomarker study of sorafenib in metastatic renal carcinoma. *J Clin Oncol*. 2008;26:4572-4578.
33. Wedam SB, Low JA, Yang SX, et al. Antiangiogenic and antitumor effects of bevacizumab in patients with inflammatory and locally advanced breast cancer. *J Clin Oncol*. 2006;24:769-777.

Figure legends

Figure 1: Example of a 78-year-old male with an intermediately differentiated adenocarcinoma of the sigmoid ($T_3N_1M_1$) with metachronous liver metastases. Left top to bottom: conventional T_1 -weighted MRI (before Gd-DTPA), fused parametric image of k_{ep} values with T_1 -weighted MRI. Right top to bottom: FDG-PET uptake image (20-50 min post injection) and parametric image of MR_{glic} . DCE-MRI: Dynamic Gd-DTPA Contrast Enhanced MRI.

Tables

Table 1: Patient characteristics	
Number of patients	23
<i>Demographic:</i> - Mean age [range] (year) - Number of men	61.5 [44.8-78.9] 17 (74%)
<i>Matched lesions per patient:</i> - Mean number [range] - Patients >1 matched lesion (%) - Median lesion MAD [IQR]	1.3 [1-5] 5 (22%) 56 mm (38-75)
<i>Histology:</i> - Adenocarcinoma - Mucinous adenocarcinoma	22 (96%) 1 (4%)
<i>Location primary tumor (%):</i> - Sigmoid - Rectum - Colon - Colon and rectum	9 (39%) 6 (26%) 5 (22%) 3 (13%)
<i>Presenting stage (%):</i> - Stage II - Stage III - Stage IV	3 (13%) 4 (17%) 16 (70%)
IQR: Interquartile Range; MAD: sum of maximal axial diameters as measured on T ₁ -weighted MRI.	

Table 2: Predictive value of pre-treatment parameters to survival assessed by Cox regression analysis.

	OS			PFS		
	HR	CI	p	HR	CI	p
Univariate:						
MR_{glc}*	3.61	1.58-8.26	0.002 [§]	3.11	1.41-6.86	0.005 [§]
MAD[†]	1.03	1.00-1.06	0.032 [§]	1.03	1.0-1.07	0.039 [§]
Chemotherapy line[‡]	2.19	0.87-5.51	0.097	2.40	0.96-6.03	0.062
Multivariate:						
MR_{glc}*	4.29	1.72-10.67	0.002 [§]	3.19	1.39-7.35	0.006 [§]
MAD[†]	1.04	1.01-1.07	0.020 [§]	1.03	1.00-1.07	0.059
Chemotherapy line[‡]	-	-	-	-	-	-

OS: overall survival; PFS: progression free survival; HR: Hazards ratio for death or progression; CI: 95% confidence interval; MR_{glc}: glucose metabolic rate; MAD: sum of maximal axial diameters as measured on T₁-weighted MRI. *per 0.1 μmol·mL⁻¹·min⁻¹ change; †per five millimeter change; §significant (p>0.05) assessed by Wald's χ² test; ‡first line versus higher lines.

Table 3: Baseline and follow-up values of vascular and metabolic parameters (n=23 patients).

	Median baseline [IQR]	Median Follow-up [IQR]	p
DCE-MRI:			
- k _{ep} (s ⁻¹)	0.014 [0.005-0.034]	0.022 [0.012-0.049]	0.056
- K ^{trans} (s ⁻¹)	0.009 [0.003-0.020]	0.016 [0.008-0.033]	0.035*
- v _e	0.638 [0.516-0.698]	0.614 [0.566-0.744]	0.893
FDG-PET:			
- MR _{glc} (μmol·mL ⁻¹ ·min ⁻¹)	0.128 [0.108-0.160]	0.054 [0.041-0.122]	<0.001*
T₁-MRI:			
- MAD (mm)	56 [50-92]	54 [47-109]	0.268

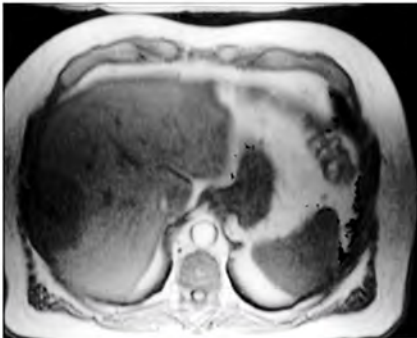
IQR: interquartile range; DCE-MRI: dynamic contrast enhanced magnetic resonance imaging; k_{ep}: rate constant between extravascular extracellular space and blood plasma; K^{trans}: volume transfer constant; v_e: volume of contrast extravascular extracellular space per unit volume of tissue; FDG-PET: [¹⁸F]-fluoro-2-deoxy-D-glucose positron emission tomography; MR_{glc}: glucose metabolic rate; MAD: sum of maximal axial diameters as measured on T₁-weighted MRI. p<0.05 (Wilcoxon signed ranks test for paired samples).

Table 4: Predictive value of therapy induced parameter changes for early response evaluation, assessed by Cox regression analysis.

	OS			PFS		
	HR	CI	p [†]	HR	CI	p [†]
Univariate:						
ΔMR_{glc} (all in FoV) [*]	1.15	1.01-1.32	0.041	-	-	-
ΔMAD [*]	1.40	1.06-1.85	0.023	1.34	1.04-1.74	0.026
Chemotherapy line [§]	-	-	-	-	-	-
Multivariate:						
ΔMR_{glc} (all in FoV) [*]	1.22	1.05-1.41	0.008	-	-	-
Δk_{ep} [*]	0.99	0.98-1.00	0.100	-	-	-
ΔMAD [*]	-	-	-	1.48	1.10-1.99	0.010
Chemotherapy line [§]	-	-	-	3.15	1.17-8.49	0.023

OS: overall survival; PFS: progression free survival; HR: Hazards ratio for death or progression; CI: 95% confidence interval; MR_{glc} : glucose metabolic rate; all in FoV: estimated including all lesions in field of view of PET-scanner; MAD: sum of maximal axial diameters as measured on T₁-weighted MRI. ^{*}per ten percent change; [†]significance assessed by Wald's χ^2 test; [§]first line versus higher lines.

DCE MRI



^{18}F -FDG PET

